

'Kondo state' and Kondo resonance in a two-dimensional electron gas

Stefan Müllegger,* Mohammad Rashidi, Michael Fattinger, and Reinhold Koch
Institute of Semiconductor and Solid State Physics, Johannes Kepler University, Linz, Austria.

The delicate balance of spin-screening and spin-aligning interactions determines many of the peculiar properties of dilute magnetic systems. We study a surface-supported all-organic multi-impurity Kondo spin system at the atomic scale by low-temperature scanning tunnelling microscopy and -spectroscopy. The model system consists of spin-1/2 radicals that are aligned in one-dimensional chains and interact *via* a ferromagnetic RKKY interaction mediated by the 2DEG of the supporting substrate. Due to the RKKY-induced enhanced depopulation of one spin-subband in the 2DEG, we finally succeeded to detect the so far unobserved 'Kondo state' as opposed to the well-established Kondo resonance. Its cloud of screening electrons, that are virtually bound to the radicals below the Kondo temperature, represents the extended exchange hole of the ferromagnetically polarized spin chain imaged here in real space.

The interaction of localized electron spins of magnetic impurities with delocalized conduction electrons provides a key handle for controlling the spin polarization in diluted magnetic systems essential for future spintronics^{1,2} and molecular electronics³ applications. Many of their unique properties are determined by the competition between screening of local spins and magnetic interactions of neighbouring spins. Below a characteristic temperature the impurity spin may be screened by a collective of conduction electrons with opposite spin – a phenomenon known as the Kondo effect⁴. The screening electrons form a virtual bound singlet many-body quantum state with the singly occupied impurity⁵ denoted herein as the 'Kondo state'³. At higher impurity concentrations, *i. e.* at sufficiently small separations, their individual Kondo states may overlap, causing an additional magnetic RKKY⁶-type interaction of individual impurity spins⁷ that competes with Kondo screening.

Recently, the study of single impurity spins on atomic scale has become a reality by means of electron transport through lateral quantum-dots^{8–10} formed in a two-dimensional electron gas (2DEG) as well as surface-supported *d*-metal impurities^{11–13} or metal-organic molecules^{14,15} inside the tunnel junction of a scanning tunnelling microscope (STM). Studies of single Kondo impurities typically report a resonance observed in the electron transmission spectrum near the Fermi energy, E_F ,¹⁶ which is commonly rationalized by the Anderson single-impurity model¹⁷ of localized magnetic states in metals [see detailed description of Fig. 1]. Already in earlier work¹⁸ the resonance signal was utilized for obtaining spatial information on the 'Kondo screening cloud'^{19,20}, *i. e.* the spatial region captured by the screening electrons surrounding the impurity. While the Kondo resonance involves only conduction electrons (near E_F), the virtual bound screening state (=Kondo state) is formed by all electrons screening the localized spin, *i. e.* the conduction electrons near E_F as well as deeper lying band electrons. A direct detection of the complete screening cloud (exchange hole) representing the Kondo state itself, has remained elusive until now.

Here we report on a low-temperature STM study of surface-supported dimers and chains of the organic

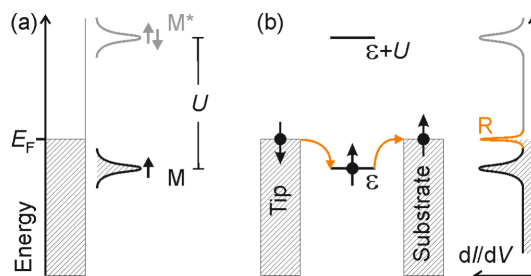


Figure 1. Kondo resonance. (a) Energy level configuration of the Anderson single-impurity model¹⁷. In this model the energy ϵ of the magnetic impurity level (M) is assumed to lie sufficiently far below E_F so that its occupation probability p is close to one, thus avoiding mixed valency ($p < 1$). Double occupation of the impurity level costs the Coulomb charging energy U and raises this state to M^* well above E_F , thus making addition of a second electron energetically unfavourable. In the bulk of metals containing dilute magnetic impurities the Kondo effect gives rise to a higher density of states⁵ for conduction electrons with opposite spin localized at the impurity sites. As a result the scattering cross-section for the conduction electrons is increased, which explains the resistivity increase of bulk Kondo systems below the Kondo temperature T_K ⁴. (b) In the case of tunnelling transport the low-lying impurity state opens up a new transport channel close to E_F ^{3,16,21,22}. Whenever an electron tunnels off the impurity, leaving behind an empty virtual intermediate state, it is replaced almost instantaneously by a conduction electron of opposite spin as demanded by the high occupation probability close to one. The extra transport channel increases²³ the transmission (conductance dI/dV) close to E_F and is commonly denoted Kondo resonance (R) in the literature^{3,16}.

⁴⁷ *sp* radical BDPA (α,γ -bisdiphenylene- β -phenylallyl,
⁴⁸ $C_{33}H_{22}$) [Fig. 2a], which is a well-established spin-1/2
⁴⁹ standard in electron spin resonance spectroscopy²⁴. We
⁵⁰ finally succeeded to tunnel out of the Kondo state it-
⁵¹ self and thus were able to detect and directly visual-
⁵² ize the exchange hole^{25,26} generated by a linear chain
⁵³ of molecular Kondo impurities in a 2DEG. In the present
⁵⁴ work, experimental detection of the Kondo state is en-
⁵⁵ abled by a remarkably strong change in conductance fa-

56 cilitated by the exceptional combination of properties
 57 of our Kondo system – as opposed to atomic d -metal
 58 Kondo systems in the literature: (i) Weak physisorp-
 59 tion of the radicals on the substrate preserves their mag-
 60 netic state. (ii) The reconstructed (111) surface of Au
 61 provides the crucial combination of surface anisotropy
 62 (herringbone reconstruction) together with a Shockley-
 63 type surface state near E_F . The former guides the self-
 64 assembly of structurally well-ordered BDPA chains and
 65 the latter acts as a 2DEG capable of communicating the
 66 Kondo effect over large distances of more than a nanome-
 67 tre across the sample surface (typical for coinage metal
 68 (111) surfaces^{18,27,28}). Thus individual Kondo states of
 69 neighbouring BDPAs are allowed to overlap. (iii) Since
 70 the singly occupied highest molecular orbital (SOMO)
 71 of BDPA is symmetry-compatible with the sp wave func-
 72 tions of the 2DEG, constructive interaction of neighbour-
 73 ing spins is facilitated. (iv) The radical-radical separation
 74 in BDPA chains on Au(111) is appropriate to give rise to
 75 an additional ferromagnetic^{7,29} RKKY-type interaction
 76 of individual BDPA spins, preferentially mediated by the
 77 2DEG, as well. (v) The resulting constructive super-
 78 position of individual Kondo states leads to an effective
 79 depopulation of one spin-subband and thus an enhance-
 80 ment of the conductance change enabling detection of the
 81 joint Kondo state by the STM tip.

BDPA self-assembly on Au(111)

83 The STM topograph of Fig. 2b reveals the forma-
 84 tion of benzene-free BDPA nanostructures upon depo-
 85 sition onto Au(111) at 300 K. Individual BDPA radi-
 86 cals are imaged as bean-shaped protrusions [see also in-
 87 set of Fig. 2c]. Pronounced clustering dominates already
 88 at submonolayer coverages, and dimers of BDPA consti-
 89 tute the smallest clusters. Larger BDPA nanostructures
 90 exhibit characteristic star-like shapes consisting of three
 91 branches of one-dimensional BDPA chains up to several
 92 nanometres long (depending on coverage). Single BDPAs
 93 are rarely observed on the surface due to an increased sur-
 94 face mobility even at 5 K, which strongly constrains the
 95 energy range accessible by STS compared to dimers and
 96 chains. As determined from STM topographs, BDPAs in
 97 chains pack closer (0.73 nm) than in dimers (0.8–0.9 nm).
 98 In the bulk phase BDPA is a one-dimensional paramag-
 99 net above 1.7 K²⁴ forming similar linear chains with a sig-
 100 nificantly larger radical-radical spacing of 1.4 nm along
 101 the \vec{b} crystallographic direction.

Kondo resonance

103 The unpaired electron of BDPA resides in the SOMO
 104 that derives from sp hybrid orbitals and is delocal-
 105 ized over the fluorene units of the molecular backbone
 106 [Fig. 2a]. When the STM tip is located over BDPA
 107 adsorbed on Au(111), typical dI/dV spectra exhibit a

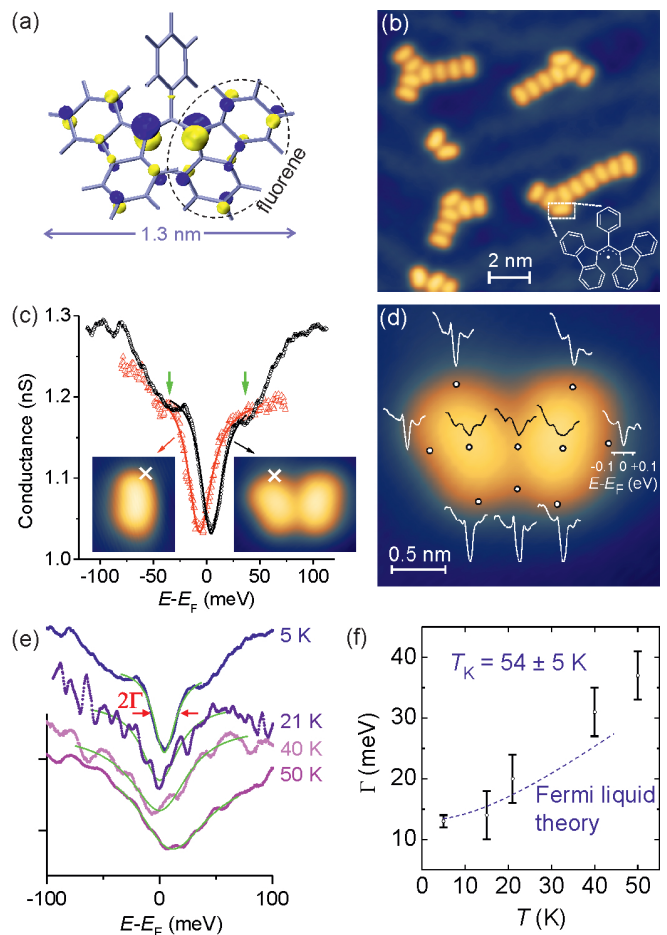


Figure 2. **BDPA on Au(111)**. (a) Chemical structure and DFT-calculated SOMO spin density of BDPA; the two ‘hot spots’ are centred around the meso-carbons. (b) STM topograph of self-assembled BDPA clusters on the Au(111) surface (+20 mV, 200 pA). (c) dI/dV spectrum of a single BDPA radical (red) and a dimer (black); the zero-bias conductance of the pristine Au(111) background at the Fermi level was calibrated to about 1.3 nS; solid lines are numerical Fano fits of Kondo antiresonance (see also Tab. I); green arrows mark vibrational satellites; insets show STM topographs of single BDPA and dimer; crosses mark the STM tip position for recording dI/dV spectrum. (d) dI/dV Kondo spectra over different positions (o) of a BDPA dimer. (e) dI/dV Kondo spectra of a BDPA dimer at different temperatures. (f) Temperature-dependent broadening; dashed line represents best-fit based on formalism of Nagaoka *et al.*³⁰.

TABLE I. Fano fit parameters of the BDPA monomer (average of four), dimer (average of three), and chain (average of three) adsorbed on Au(111) at 5 K; asymmetry parameter q , resonance position ΔE and half-width Γ .

	$q (\pm 0.1)$	$\Delta E (\pm 0.7 \text{ meV})$	$\Gamma (\pm 1 \text{ meV})$
monomer	-0.15	-5.9	11
dimer	-0.23	+2.3	13
chain	-0.15	+7.0	19

108 strong conductance minimum (dip) close to E_F [Fig. 2c].
 109 The maximum amplitude is observed for tip positions
 110 near the rim of BDPA, while over intramolecular posi-
 111 tions the dip broadens and decreases [Fig. 2d]. The dip
 112 amplitude amounts to more than 20% of the zero-bias
 113 conductance of the pristine substrate for our best STM
 114 tips. We observe almost identical spectra for BDPA rad-
 115 icals adsorbed over different fcc and elbow positions of
 116 the reconstructed Au(111) surface, suggesting that the
 117 adsorption site relative to the substrate atomic lattice is
 118 negligible. A detailed analysis of our STS results confirms
 119 the characteristic properties of the transmission Kondo
 120 effect^{11,12} for BDPA/Au(111): (i) The conductance min-
 121 imum lies within a few milli-electronvolts around E_F . (ii)
 122 The resonance width, 2Γ , increases with temperature and
 123 the amplitude decreases simultaneously [Figs. 2e,f]. (iii)
 124 The spectral shape of the dip²³ is well described by the
 125 Fano function^{21,31,32} [Fig. 2c]; the numerical values of
 126 the fit parameters are listed in Tab. I. (iv) The reso-
 127 nance is accompanied by two satellite features symmet-
 128 rically offset around the Kondo dip [marked by green
 129 arrows in Fig. 2c] indicating molecular vibrations exci-
 130 cated by inelastic tunnelling processes. This is expected
 131 for molecule-based Kondo systems where the impurity
 132 orbital (SOMO) is spatially extended and thus sensi-
 133 tive to geometric changes of the molecular backbone³³.
 134 The respective vibrational energy of $\approx 35\text{--}55$ meV (300–
 135 450 cm^{-1}) points to one or more collective vibrational
 136 modes of the BDPA backbone rather than plain C-H vi-
 137 brations, which are typically observed at higher energies
 138 as suggested by our density functional theory (DFT) cal-
 139 culations.

140 The lower surface mobility of BDPA dimers compared
 141 to single radicals facilitates recording of the Kondo res-
 142 onance width up to temperatures of 50 K [Fig. 2f].
 143 The respective broadening is analysed in detail based
 144 on a Fermi liquid description put forward by Nagaoka
 145 *et al.*³⁰. The least-square fit based on this formalism,
 146 $\Gamma = 2\sqrt{(\pi k_B T)^2 + 2(k_B T_K)^2}$, is shown as dashed curve
 147 in Fig. 2f. The obtained nominal value of $T_K = 54 \pm 5$ K is
 148 consistent with the resonance width of $2k_B T_K$ predicted
 149 by Fermi liquid theory. [For further details on the Kondo
 150 signal of BDPA/Au(111) see Supplementary Information
 151 S1.]

152 The existence of a Kondo signal corroborates that
 153 BDPA preserves the magnetic ground state after adsorp-
 154 tion on Au(111) at the single radical level. Our elec-
 155 tron spin resonance (ESR) experiments on samples with
 156 BDPA monolayer coverage on Au(111)/mica substrates
 157 yield $g = 1.96$ at 7 K. This value is in good agreement
 158 with that of the single-crystal bulk phase (2.0026)³⁴ as
 159 well as that observed in ultrathin BDPA films drop-cast
 160 on Au(111) substrates (2.005)³⁵ at room temperature.
 161 Both, Kondo behaviour and ESR signal, evidence that
 162 a possible charge transfer between BDPA and the Au
 163 substrate is very small.

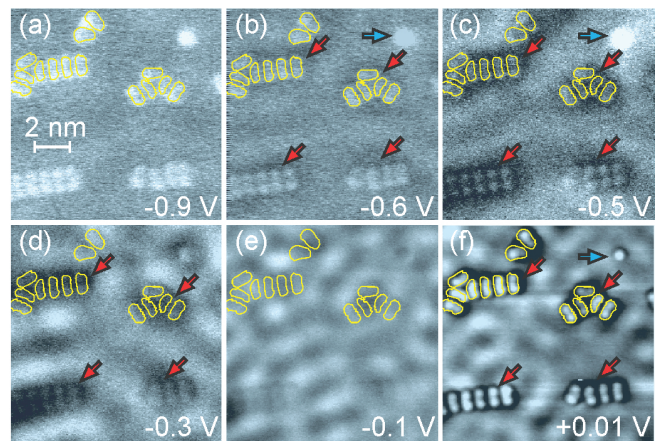


Figure 3. **Spectroscopic dI/dV maps at different bias voltages.** Overlaid yellow contour lines mark areas covered by BDPA molecules as extracted from STM topographs; red arrows indicate reduced-conductance envelopes, blue arrows a surface defect.

Experimental observation of the Kondo state

165 The spectroscopic images of Fig. 3 reveal intriguing
 166 details of the Kondo screening of BDPA clusters on
 167 Au(111). Doubly occupied pure MO states [see Supple-
 168 mentary Information S2] are imaged as bright protrusions
 169 confined to the area covered by the BDPA molecules
 170 [Fig. 3a]. For sample bias ranging from about -0.6 to
 171 -0.3 V we observe areas of reduced conductance (dark)
 172 enveloping the BDPA clusters as marked by red arrows
 173 in Figs. 3c,d. These areas clearly extend more than 1 nm
 174 into regions of the pristine Au(111) surface outside of
 175 and in between neighbouring BDPAs – in clear contrast
 176 to the pure MO states of Fig. 3a. We denote them as
 177 reduced-conductance envelopes (RCEs), since dI/dV is
 178 reduced by about 50% relative to zero-bias conductance
 179 of the pristine Au(111) surface. The RCEs start to ap-
 180 pear slightly below the onset of the Au(111) surface-state
 181 band close to -0.5 V [Figs. 3b,c]. They persist over an
 182 energy range of about 200 meV [Fig. 3d] and fade off when
 183 further approaching zero bias. Above -0.3 V the pristine
 184 standing-wave pattern of the surface state electrons is
 185 imaged [Fig. 3e]. It originates from scattering at the her-
 186 ringbone reconstruction pattern³⁶ of the Au(111) surface
 187 and the BDPA clusters. In the standing wave pattern
 188 of Fig. 3e we find no evidence for an enhanced electro-
 189 static scattering potential localized at the BDPA radicals
 190 (which are hardly visible). This evidences³⁷ that the ad-
 191 sorbed radicals have (almost) zero total charge – in agree-
 192 ment with our ESR results. Even with the STM tip above
 193 BDPA the characteristic step-like conductance signal of
 194 the surface state survives almost unaffected [see Figure
 195 S1 of the Supplementary Information]. This indicates
 196 that hybridization of BDPA orbital(s) with the surface
 197 state is only weak and, in particular, rules out that the
 198 observed RCEs originate from a possible localization³⁸

199 of the surface state. The possibility that local inter-
 200 ference minima of the elastically scattered surface-state
 201 electron waves would cause the observed RCEs is cer-
 202 tainly ruled out^{39,40}, as well: (i) The RCEs are absent
 203 in the surface-state standing-wave pattern of Fig. 3e. (ii)
 204 The RCEs lack any oscillating behaviour expected for
 205 scattered surface-state waves⁴¹. (iii) The RCEs are de-
 206 tected only at the BDPA units, but not at surface im-
 207 purities [marked by a blue arrow in Figs. 3b,c,f]. Possi-
 208 ble life-time effects are known to flatten the surface-state
 209 band edge typically in the order of 10 meV⁴² and thus are
 210 one order of magnitude too small to explain the observed
 211 RCEs, as well.

212 Closely around zero bias the RCEs reappear again
 213 [Fig. 3f] and represent the conductance map of the Kondo
 214 resonance measured point-by-point in Figs. 2c,d. The
 215 RCEs of Fig. 3f thus reflect the lateral spatial distri-
 216 bution of the Kondo resonance signal of BDPA clus-
 217 ters on Au(111). The sample area at which the Kondo
 218 resonance is observed by STM has been commonly at-
 219 tributed to the spatial extent of the Kondo screening
 220 cloud^{18,43}. However, the interpretation of its size re-
 221 mains a controversial matter, because it is much smaller
 222 than the Kondo screening length predicted by Fermi liq-
 223 uid theory [see Supplementary Information S3]. The
 224 Kondo dip of BDPA/Au(111) is detected more than
 225 1.5 nm laterally away from BDPA and decays according
 226 to $1/r$ [see Supplementary Information S4]. This suggests
 227 that the Kondo screening of BDPA/Au(111) strongly in-
 228 volves delocalized electronic states^{22,44} – most possibly
 229 the surface-state band of Au(111) that acts as a 2DEG.

230 Discussion: Kondo state vs. Kondo resonance

231 The additional RCEs of Figs. 3c,d observed at ener-
 232 gies well below E_F come – at first sight – as a surprise.
 233 Since the most obvious possible alternatives are ruled
 234 out above, there is strong evidence that the additional
 235 RCEs originate from the Kondo state (KS) itself, i.e.
 236 the many-body virtual bound state including the spin-
 237 screening contributions from deeper lying band electrons
 238 as well as conduction electrons near E_F . This is illus-
 239 trated in Fig. 4: (i) Their energy onset coincides remark-
 240 ably well with the band edge of the Au(111) surface-state.
 241 The latter is strongly involved in the Kondo screening of
 242 BDPA/Au(111), as indicated by our results. (ii) The ge-
 243 ometric size and shape are qualitatively similar to the
 244 RCEs of the Kondo resonance, but the signal amplitude
 245 is much stronger and they extend even further into areas
 246 of the pristine Au(111) surface [compare Figs. 3d and
 247 f]. (iii) The Kondo state involves an interaction of the
 248 surface-state and the SOMO, suggesting a similar energy
 249 range for both. This is illustrated in Fig. 4 and corrob-
 250 orated by point spectroscopy [see Supplementary Infor-
 251 mation S2].

252 The observed reduction of the tunnelling conductance
 253 is rationalized as follows: The density-of-states of the

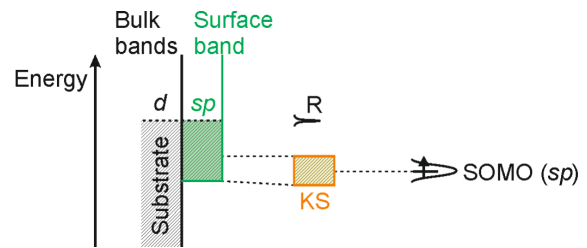


Figure 4. **Schematics summarizing the dI/dV results of BDPA/Au(111).** In addition to the Kondo resonance (R) close to E_F the Kondo state (KS) is detected experimentally via contributions from deeper lying surface-state band electrons. The Kondo state originates from resonant spin exchange processes between the magnetic impurity (SOMO of BDPA) and the surface-state band of Au(111).

254 2DEG consists of two overlaid identical step-functions⁴⁶
 255 with different Fermi wave vectors, Rashba-split in k -
 256 space⁴⁵ but having the same energy onset. Our results
 257 indicate that Kondo screening depletes one of the spin
 258 subbands in the surface area around BDPA (*e.g.* the
 259 up-spin subband if BDPA is up-spin). The decreased
 260 occupation of one subband (exchange hole) reduces the
 261 number of available electrons for tunnelling out of the
 262 surface state. The spin screening is effective not only
 263 for conduction electrons near E_F , but for deeper lying
 264 band electrons, as well. This equals an effective loss of a
 265 tunnelling transmission channel and thus a reduction of
 266 the tunnelling conductance – as evidenced by our exper-
 267 iments.

268 The dI/dV images of Figs. 3c,d corroborate that the
 269 Kondo state (*i.e.* the screening cloud) of individual
 270 BDPA radicals on Au(111) are so large that they readily
 271 overlap with those of their next neighbours. In the case
 272 of two or more neighbouring Kondo impurities an addi-
 273 tional RKKY-type indirect-exchange interaction of their
 274 spins evolves, according to predictions based on Fermi-
 275 liquid theory⁷. The RKKY interaction of neighbouring
 276 Kondo impurities is either ferromagnetic ($J_{\text{RKKY}} > 0$)
 277 or antiferromagnetic^{14,29,47,48} (< 0) and competes with
 278 Kondo screening ($J_{\text{Kondo}} < 0$) as illustrated in Fig. 5a.
 279 Similar to the Kondo screening, the RKKY interaction
 280 between BDPA radicals in chains on Au(111) is predom-
 281 inantly mediated by surface-state electrons. The sur-
 282 face band of Au(111) starts 500 meV below E_F , and
 283 has a Fermi wave number of $k_F^{-1} = 0.617$ and 0.540 nm
 284 including the Rashba splitting⁴⁵. A possible coupling
 285 mediated by bulk conduction electrons decays at much
 286 shorter distances due to the smaller $k_F^{-1} = 0.08$ nm⁴⁵
 287 and thus is negligible for intermolecular interactions in
 288 BDPA clusters. A calculation of the distance-dependent
 289 oscillation of the RKKY coupling constant for the two-
 290 dimensional case⁴⁹ based on the momentum and effec-
 291 tive mass ($m^* = 0.25m_0$)⁴⁵ of the Au(111) surface state
 292 yields a ferromagnetic RKKY interaction for separations
 293 smaller than 1 nm. Thus, for next-neighbour BDPA rad-

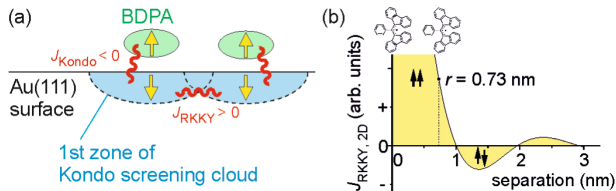


Figure 5. **Competition of RKKY and Kondo interaction.** (a) Schematics illustrating the overlap of the Kondo clouds of two neighbouring BDPA radicals adsorbed on the Au(111) surface. (b) Calculated separation-dependent oscillatory behaviour of the two-dimensional RKKY coupling constant $J_{\text{RKKY},2\text{D}}$ for $k_{\text{F}}^{-1} = 0.614$ nm.

icals in chains, which are separated by 0.73 nm, a parallel spin alignment is favoured as illustrated in Fig. 5b. Ferromagnetic RKKY facilitates a constructive superposition of individual Kondo states, which enhances the depopulation of one subband and, consequently, further lowers the conductance for tunnelling out of the surface-state. This enhancement effect seems to be essential for enabling experimental detection of the Kondo state. Since the RKKY interaction strength decays with $1/r^3$, the influence of the next-neighbour BDPA is dominant in BDPA chains. Thus BDPA chains on Au(111) are expected to be paramagnetic at 5 K in agreement with our results as well as a recent ESR study³⁵.

Tunneling out of the Kondo state is further supported by the fact that the molecules are weakly imaged by STS between -0.7 and -0.5 V but not at -0.1 V.

In dimers the radical-radical separation of 0.8–0.9 nm is larger and close to the transition between ferro- and antiferromagnetic alignment [Fig. 5]. Consequently, the RKKY-based enhancement effect for the Kondo state signal of BDPA dimers is decreased – consistent with our results [Fig. 3c,d]. In the case of the mobile monomers, we did not succeed to detect the Kondo state, although the Kondo resonance close to E_{F} is clearly observed [Fig. 3f]. This is consistent with the absence of a RKKY-based enhancement effect in monomers. The interaction between neighbouring radicals in the chains is observed to affect the width of the spectral Kondo resonance. Table I lists the values of the resonance width, Γ , for the BDPA monomer, dimer and chain as determined from our experiments.

A. Conclusions

We succeeded to detect and image the joint Kondo state (as opposed to the Kondo resonance) of an all-

organic multi-impurity Kondo system at the atomic scale. Our Kondo system consists of spin-1/2 radicals that are aligned in one-dimensional chains and ferromagnetically coupled *via* RKKY interaction mediated by the 2DEG of the supporting substrate. The related cloud of screening electrons with opposite spin and virtually bound to the radicals below the Kondo temperature represents the extended exchange hole of the ferromagnetically coupled spin chain. Our achieved mapping of the Kondo state utilizes the RKKY-enhanced depopulation of one spin subband in the 2DEG and opens a new way to study magnetic interactions of spin-carrying molecules in coupled spin clusters with impact on the development of molecular-based magnetic logic applications for future spin- and molecular electronics.

Methods

BDPA recrystallized in benzene was thermally evaporated in ultrahigh vacuum (UHV) from a quartz crucible at 383 K after thorough degassing at 373 K. The single-crystal Au(111) surface was prepared by repeated cycles of 0.5 keV Ar^+ bombardment and annealing at 720 K. STM and STS experiments were carried out at 7 K employing electrochemically etched W tips. The dI/dV signal was obtained from the first-harmonic current signal detected by lock-in technique (0.5–2 kHz; 5–20 mV sinusoidal peak-to-peak voltage; average of 10 single spectra). W tips were deoxidized by annealing in UHV; impurity- and tip effects were minimized by careful sample preparation and multiple tip formings between the dI/dV experiments, resulting in Au-coated STM tips. Reliable tip performance was established by accurately reproducing the dI/dV signature of the Au(111) surface state from literature³⁶. dI/dV spectra were recorded at constant-height conditions, the spectroscopic images (dI/dV maps) simultaneously with constant-current STM topographic imaging. Gas-phase density functional theory (DFT) single point energy calculations were performed with Gaussian 03 package⁵⁰ using B3LYP hybrid functional⁵¹, 6-31G(d) basis set and fixed molecular geometry extracted from BDPA bulk crystal structure⁵².

References

¹ Wolf, S. A. *et al.* Spintronics: A spin-based electronics vision for the future. *Science* **294**, 1488–1495 (2001).

* stefan.muellegger@jku.at

- 2 Nature milestones in spin. *Nature Phys.* **4**, S5–S20 (2008). 437
- 3 Scott, D. G. & Natelson, D. Kondo resonances in molecular devices. *ACS Nano* **4**, 3560–3579 (2010). 438
- 4 Kondo, J. Resistance minimum in dilute magnetic alloys. *Prog. Theor. Phys.* **32**, 37 (1964). 439
- 5 Hewson, A. C. *The Kondo Problem to Heavy Fermions* (Cambridge University Press, Cambridge, 1993). 440
- 6 Kittel, C. *Solid State Physics*, vol. 22 (Academic, New York, 1968). 441
- 7 Simon, P., Lopez, R. & Oreg, Y. Ruderman-Kittel-Kasuya-Yosida and magnetic-field interactions in coupled Kondo quantum dots. *Phys. Rev. Lett.* **94**, 086602 (2005). 442
- 8 Goldhaber-Gordon, D. *et al.* Kondo effect in a single-electron transistor. *Nature* **391**, 156–159 (1998). 443
- 9 Cronenwett, S. M., Oosterkamp, T. H. & Kouwenhoven, L. P. A tunable Kondo effect in quantum dots. *Science* **281**, 540–544 (1998). 444
- 10 Jeong, H., Chang, A. M. & Melloch, M. R. The Kondo effect in an artificial quantum dot molecule. *Science* **293**, 2221–2223 (2001). 445
- 11 Li, J., Schneider, W. D., Berndt, R. & Delley, B. Kondo scattering observed at a single magnetic impurity. *Phys. Rev. Lett.* **80**, 2893–2896 (1998). 446
- 12 Madhavan, V., Chen, W., Jamneala, T., Crommie, M. F. & Wingreen, N. S. Tunneling into a single magnetic atom: Spectroscopic evidence of the Kondo resonance. *Science* **280**, 567 (1998). 447
- 13 Ternes, M., Heinrich, A. J. & Schneider, W. D. Spectroscopic manifestations of the Kondo effect on single adatoms. *J. Phys.: Condens. Matter* **21**, 05300 (2009). 448
- 14 Iancu, V., Deshpande, A. & Hla, S. Manipulation of the Kondo effect via two-dimensional molecular assembly. *Phys. Rev. Lett.* **97**, 266603 (2006). 449
- 15 Gao, L. *et al.* Site-specific Kondo effect at ambient temperatures in iron-based molecules. *Phys. Rev. Lett.* **99**, 106402 (2007). 450
- 16 Wingreen, N. S. The Kondo effect in novel systems. *Mater. Sci. Eng. B* **84**, 22–25 (2001). 451
- 17 Anderson, P. W. Localized magnetic states in metals. *Phys. Rev.* **124**, 41–53 (1961). 452
- 18 Manoharan, H. C., Lutz, C. P. & Eigler, D. M. Quantum mirages formed by coherent projection of electronic structure. *Nature* **403**, 512–515 (2000). 453
- 19 Affleck, I. & Simon. Detecting the Kondo screening cloud around a quantum dot. *Phys. Rev. Lett.* **86**, 2854–2857 (2001). 454
- 20 Affleck, I., Borda, L. & Saleur, H. Friedel oscillations and the Kondo screening cloud. *Phys. Rev. B* **77**, 180404 (2008). 455
- 21 Ujsaghy, O., Kroha, J., Szunyogh, L. & Zawadowski, A. Theory of the Fano resonance in the STM tunneling density of states due to a single Kondo impurity. *Phys. Rev. Lett.* **85**, 2557–2560 (2000). 456
- 22 Plihal, M. & Gadzuk, J. W. Nonequilibrium theory of scanning tunneling spectroscopy via adsorbate resonances: Nonmagnetic and Kondo impurities. *Phys. Rev. B* **63**, 085404 (2001). 457
- 23 We remark that in STM experiments, often a dip is observed instead of a peak, i.e. a Kondo antiresonance (= decreased transmission). This is explained by quantum interference of direct and indirect tunnelling paths. Accordingly, the Kondo resonance has a Fano line-shape³¹ determined by an asymmetry factor q that depends on the ratio t_2/t_1 of transmission amplitudes of the respective paths^{21,22,32}. 458
- 24 Duffy, W. *et al.* Antiferromagnetic linear chains in the crystalline free radical BDPA*. *J. Chem. Phys.* **56**, 2555–2561 (1972). 459
- 25 Schumann, F. O., Kirschner, J. & Berakdar, J. Mapping out electron-electron interactions at surfaces. *Phys. Rev. Lett.* **95**, 117601 (2005). 460
- 26 Schumann, F. O. *et al.* Spin-resolved mapping of spin contribution to exchange-correlation holes. *Phys. Rev. Lett.* **104**, 087602 (2010). 461
- 27 Henzl, J. & Morgenstern, K. Contribution of the surface state to the observation of the surface Kondo resonance. *Phys. Rev. Lett.* **98**, 266601 (2007). 462
- 28 Li, Q. *et al.* Direct evidence of the contribution of surface states to the Kondo resonance. *Phys. Rev. B* **80**, 115431 (2009). 463
- 29 Wahl, P. *et al.* Exchange interaction between single magnetic adatoms. *Phys. Rev. Lett.* **98**, 056601 (2007). 464
- 30 Nagaoka, K., Jamneala, T., Grobis, M. & Crommie, M. F. Temperature dependence of a single Kondo impurity. *Phys. Rev. Lett.* **88**, 077205 (2002). 465
- 31 Fano, U. Effects of configuration interaction on intensities and phase shift. *Phys. Rev.* **124**, 1866–1878 (1961). 466
- 32 Figgins, J. & Morr, D. K. Differential conductance and quantum interference in Kondo systems. *Phys. Rev. Lett.* **104**, 187202 (2010). 467
- 33 Fernandez-Torrente, I., Franke, K. J. & Pascual, J. I. Vibrational Kondo effect in pure organic charge-transfer assemblies. *Phys. Rev. Lett.* **101**, 217203 (2008). 468
- 34 Hamilton, W. O. & Pake, G. E. Linear Antiferromagnetism in the Organic Free Radical 1,3Bisdiphenylene2 Phenyl Allyl. *J. Chem. Phys.* **39**, 2694–2697 (1963). 469
- 35 Messina, P. *et al.* Spin noise fluctuations from paramagnetic molecular adsorbates on surfaces. *J. Appl. Phys.* **101**, 053916 (2007). 470
- 36 Bürgi, L., Brune, H. & Kern, K. Imaging of electron potential landscapes on Au(111). *Phys. Rev. Lett.* **89**, 176801 (2002). 471
- 37 Olsson, F. E., Paavilainen, S., Persson, M., Repp, J. & Meyer, G. Multiple Charge States of Ag Atoms on Ultrathin NaCl Films. *Phys. Rev. Lett.* **98**, 176803 (2007). 472
- 38 Limot, L., Pehlke, E., Kröger, J. & Berndt, R. Surface-State Localization at Adatoms. *Phys. Rev. Lett.* **94**, 036805 (2005). 473
- 39 Crommie, M. F. Observing electronic scattering in atomic-scale structures on metals. *J. El. Spec. Rel. Phen.* **109**, 1–17 (2000). 474
- 40 Schneider, M. A. *et al.* Kondo state of Co impurities at noble metal surfaces. *Appl. Phys. A: Mat. Sci. & Proc.* **80**, 937–941 (2005). 475
- 41 Gross, L. *et al.* Scattering of surface state electrons at large organic molecules. *Phys. Rev. Lett.* **93**, 056103 (2004). 476
- 42 Schneider, W. D. & Berndt, R. Low-temperature scanning tunneling spectroscopy: Kondo effect and surface state lifetimes. *J. El. Spec. Rel. Phen.* **109**, 19–31 (2000). 477
- 43 Prüser, H. *et al.* Long-range Kondo signature of a single magnetic impurity. *Nature Phys.* **7**, 203–206 (2011). 478
- 44 Knorr, N., Schneider, M. A., Diekhöner, L., Wahl, P. & Kern, K. Kondo effect of single Co adatoms on Cu surfaces. *Phys. Rev. Lett.* **88**, 096804 (2002). 479
- 45 Reinert, F. Spin-orbit interaction in the photoemission spectra of noble metal surface states. *J. Phys.: Condens. Matter* **15**, S693–S705 (2003). 480
- 46 Datta, S. *Quantum Transport: Atom to Transistor* (Cambridge University Press, Cambridge, 2005). 481

- 501 ⁴⁷ Tsukahara, N. *et al.* Evolution of Kondo resonance from
 502 a single impurity molecule to the two-dimensional lattice.
 503 *Phys. Rev. Lett* **106**, 187201 (2011).
 504 ⁴⁸ Bork, J. *et al.* A tunable two-impurity Kondo system in
 505 an atomic point contact. *Nature Phys.* **7**, 901–906 (2011).
 506 ⁴⁹ Beal-Monod, M. T. Ruderman-Kittel-Kasuya-Yosida indi-
 507 rect interaction in two dimensions. *Phys. Rev. B* **36**, 36–37
 508 (1987).
 509 ⁵⁰ M. J. Frisch *et al.* Gaussian 03, Revision E.01 Gaussian,
 510 Inc., Wallingford, CT, 2004.
 511 ⁵¹ Becke, A. D. Density-functional thermochemistry. III. the
 512 role of exact exchange. *J. Chem. Phys.* **98**, 5648 (1993).
 513 ⁵² Azuma, N., Ozawa, T. & Yamauchi, J. Molecular and
 514 crystal structures of complexes of stable free radical BDPA
 515 with benzene and acetone. *Bull. Chem. Soc. Jpn.* **67**, 31–
 516 38 (1994).

Acknowledgements

517
 518 We thank Wolfgang Jantsch at Johannes Kepler Uni-
 519 versity for the EPR investigations and Andreas Ney for

520 stimulating discussion. Financial support by the Aus-
 521 trian Science Fund (FWF project P20773) is acknowl-
 522 edged.

Author contributions

523
 524 S.M., M.R. and M.F. carried out experiments. S.M.
 525 and M.R. analyzed the data. S.M. and R.K. wrote the
 526 manuscript, planned and supervised the project. All au-
 527 thors discussed the manuscript.

Additional information

528
 529 The authors declare no competing financial inter-
 530 ests. Supplementary information accompanies this
 531 paper on www.nature.com/naturephysics. Reprints
 532 and permissions information is available online at
 533 <http://www.nature.com/reprints>. Correspondence and
 534 requests for materials should be addressed to S.M.

Supplementary information: Kondo state and Kondo resonance in a two-dimensional electron gas

Stefan Müllegger,* Mohammad Rashidi, Michael Fattinger, and Reinhold Koch
Institute of Semiconductor and Solid State Physics, Johannes Kepler University, Linz, Austria.

S1. Details of the Kondo resonance of BDPA/Au(111)

The shape of the Kondo resonance is determined by the phase between different tunneling paths (into the Fermi sea or into the impurity level) and the particle-hole symmetry of the conduction band¹. The observation of a dip (reduced conductance) rather than a peak is reflected by the numerical value of the asymmetry parameter q in the fitted Fano-lineshape. q depends on the ratio of tunneling amplitudes for different possible tunneling paths^{2,3}. The obtained value of $q \ll 1$ (see Table I) thus indicates predominant tunneling into the continuum of substrate states rather than the impurity state (which is here the SOMO) due to Coulomb repulsion.

The energetic position, $\Delta E = E - E_F$, of the Kondo dip is offset from the Fermi level. Both magnitude and sign of ΔE are clearly affected by the presence of a second neighbouring BDPA molecule in dimers [see Fig. 2c and Table I]. While in single BDPAs the Kondo dip lies below the Fermi level, it lies above it for dimers. A negative (positive) offset, ΔE , indicates an occupied (empty) state. Fermi-liquid theory rationalizes the offset ΔE by the asymmetric level alignment of SOMO and SUMO relative to E_F (the so-called electron-hole asymmetry⁴) determined by the occupation number of the impurity level (SOMO). Without particle-hole symmetry the SOMO occupation number becomes $\neq 1$ and the Kondo peak gets displaced relative to the Fermi level.⁴ When it is < 1 the level is less than half-full and the Kondo resonance lies above E_F and below it for > 1 .

The width of the Kondo dip increases by about 19% in dimers compared to singles (see Table I).

S2. Point spectroscopy

The energy that determines whether Kondo physics will be visible is $k_B T_K \approx 5$ meV, is always smaller than the FWHM of the impurity level⁴ (SOMO). To determine the energies and widths of SOMO and SUMO relative to the substrate Fermi level we recorded local dI/dV spectra of BDPA dimers with the STM tip positioned over BDPA near the rim (Fig. S1). The Kondo dip close to E_F is visible (red arrow) and significantly larger than the modulation ('ripples') of the surface-state band caused by the regular herringbone reconstruction of the Au(111)⁵. Typical spectra exhibit a small filled-state resonance around -0.7 to -0.9 eV and a strong empty-state resonance around $+1.5$ eV marked by black arrows. We

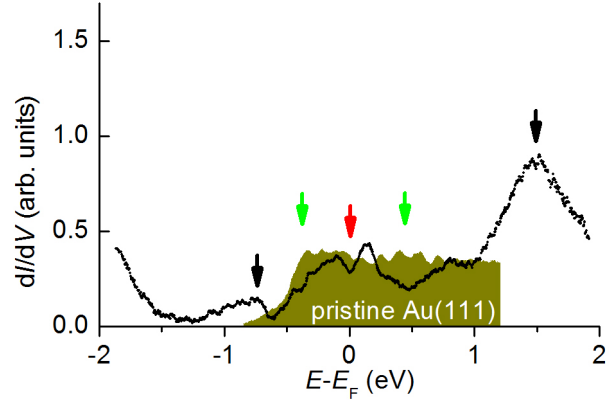


Figure S1. dI/dV spectrum with STM tip over rim of BDPA dimer; dark yellow: pristine Au(111) surface.

attribute them to the doubly occupied HOMO and doubly unoccupied LUMO-related states.

Unfortunately, no distinct SOMO/SUMO resonances are observed in the spectrum. This may be due to the steric protection of the SOMO/SUMO, which corresponds to a small tunnelling amplitude into or out of the SUMO/SOMO – the same reason as for the observed small Fano q factor (see above). Nevertheless, the positions of SOMO/SUMO can be approximated by a comparison with the spectrum of the pristine Au(111) surface in Fig. S1. Close to about ± 0.5 V the conductance of BDPA is reduced below that of the pristine substrate, suggesting two antiresonances (marked by green arrows) that relate to SOMO/SUMO. The respective SOMO-SUMO energy gap of $U \approx 1$ eV is consistent with the DFT-calculated value of $U = 1.56$ eV obtained for a single BDPA radical in the gas-phase, because a slight narrowing of the gap by a few tenths of electronvolts is commonly observed for organic molecules adsorbed on metal surfaces.

S3. Kondo screening cloud

Even the largest characteristic lengths of several nanometers^{6,7} so far obtained from experimental data are much shorter than the theoretical Kondo screening length $\xi_K = \hbar v_F / (k_B T_K)$ predicted to be about 0.1 – 1 μm (Fermi velocity $v_F = \hbar k_F / m^*$ and effective mass m^*)^{8,9}. Recent theoretical studies seem to be just about to resolve this issue, and corroborating that ξ_K plays no significant role in experimental dI/dV data, but that, rather, the experimentally observed dI/dV features decay within a few

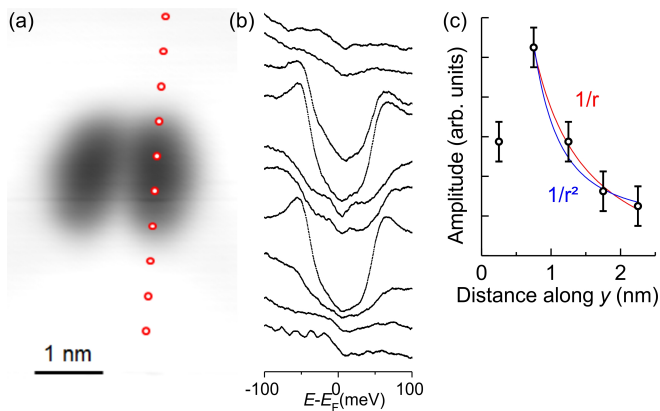


Figure S2. **Distance-dependent decay of the Kondo signal.** (a) STM topo of BDPA dimer. (b) dI/dV Kondo spectra recorded at different tip positions as marked by circles. (c) Decay of Kondo amplitude with increasing distance from BDPA; solid lines are fits of $1/r$ and $1/r^2$.

Fermi wavelengths¹⁰.

For the Au(111) surface state ($m^* = 0.25 \cdot m_0$, $k_F = 0.162 \text{ \AA}^{-1}$) a value of $\xi_K = 106 \text{ nm}$ is obtained. The diameter of our RCEs observed close to E_F are much smaller than ξ_K . (For Au bulk electrons with $v_F \approx 1.4 \cdot$

10^6 m/s one obtains a value of $\xi_K = 198 \text{ nm}$).

S4. Spatial decay of the Kondo resonance signal

Figure S2 illustrates the results of distance-dependent STS measurements along a specific high symmetry direction of a BDPA dimer. STS spectra were recorded with the STM tip over positions at increasing lateral separation from the BDPA dimer as marked by the circles in Fig. S2a. The respective spectra shown in Fig. S2b exhibit the characteristic Kondo dip even at large lateral separations of more than 1.5 nm from BDPA, while the amplitude of the dip decreases monotonically. The spatially decaying amplitude values are plotted in Fig. S2c together with the best-fit curve obtained for a decay according to $1/r$ (red curve) with a reduced $\chi^2 = 1.1$. For comparison, we fitted a $1/r^2$ decay as well (blue curve), which results in a significantly poorer agreement with the experimental data ($\chi^2 = 1.7$).

References

-
- * stefan.muellegger@jku.at
- ¹ Figgins, J. & Morr, D. K. Differential conductance and quantum interference in Kondo systems. *Phys. Rev. Lett.* **104**, 187202 (2010).
 - ² Ujsaghy, O., Kroha, J., Szunyogh, L. & Zawadowski, A. Theory of the Fano resonance in the STM tunneling density of states due to a single Kondo impurity. *Phys. Rev. Lett.* **85**, 2557–2560 (2000).
 - ³ Plihal, M. & Gadzuk, J. W. Nonequilibrium theory of scanning tunneling spectroscopy via adsorbate resonances: Nonmagnetic and Kondo impurities. *Phys. Rev. B* **63**, 085404 (2001).
 - ⁴ Hewson, A. C. *The Kondo Problem to Heavy Fermions* (Cambridge University Press, 1993).
 - ⁵ Chen, W., Madhavan, V., Jamneala, T. & Crommie, M. Scanning tunneling microscopy observation of an electronic superlattice at the surface of clean gold. *Phys. Rev. Lett.* **80**, 1469–1472 (1998).
 - ⁶ Manoharan, H. C., Lutz, C. P. & Eigler, D. M. Quantum-mirages formed by coherent projection of electronic structure. *Nature* **403**, 512–515 (2000).
 - ⁷ Prüser, H. *et al.* Long-range Kondo signature of a single magnetic impurity. *Nature Phys.* **7**, 203–206 (2011).
 - ⁸ Affleck, I. & Simon. Detecting the Kondo screening cloud around a quantum dot. *Phys. Rev. Lett.* **86**, 2854–2857 (2001).
 - ⁹ Affleck, I., Borda, L. & Saleur, H. Friedel oscillations and the Kondo screening cloud. *Phys. Rev. B* **77**, 180404 (2008).
 - ¹⁰ Büsser, C. A. *et al.* Numerical analysis of the spatial range of the Kondo effect. *Phys. Rev. B* **81**, 045111 (2010).
 - ¹¹ Reinert, F. Spin-orbit interaction in the photoemission spectra of noble metal surface states. *J. Phys.: Condens. Matter* **15**, S693–S705 (2003).
 - ¹² Ashcroft, N. W. & Mermin, N. D. *Solid State Physics* (Cengage Learning Emea, 1976).